Global Fault-Tolerant Control of Underactuated Aerial Vehicles with Redundant Actuators

Hindawi
International Journal of Aerospace Engineering
Volume 2019, Article ID 9754981, 12 pages
https://doi.org/10.1155/2019/9754981

Research Article

Global Fault-Tolerant Control of Underactuated Aerial Vehicles with Redundant Actuators

Yushu Yu [1,2] **and Yiqun Dong** [3]

[1]*Department of Mechanics and Maritime Sciences, Chalmers University of Technology, Gothenburg SE-41296, Sweden*
[2]*Robotics Institute, Beihang University, Beijing 100191, China*
[3]*Department of Mechanical Engineering, University of Michigan, Ann Arbor, MI 48109, USA*

Correspondence should be addressed to Yiqun Dong; yiqundong90@gmail.com

Received 18 June 2018; Revised 12 September 2018; Accepted 9 November 2018; Published 11 February 2019

Academic Editor: Joseph Morlier

In this paper, we consider the fault-tolerant control problem for aerial vehicles with redundant actuators. The redundant actuator brings difficulty in fault identification and isolation. Active fault-tolerant control is adopted in this paper as it can detect actuator fault. The entire proposed fault-tolerant control algorithm contains a baseline controller, the fault detection and isolation scheme, and the controller reconstruction module. A robust parameter identification method is designed to identify the torque and thrust generated by the actuators. The feasibility of isolating the fault for the redundant actuators is analyzed through mathematical proof. Through the analysis, the practical fault isolation algorithm is also proposed. Two typical aerial vehicles with redundant actuators, an eight-rotor aircraft and a hexa-rotor aircraft, are adopted in numerical simulations to verify the effectiveness of the proposed fault-tolerant control approach.

1. Introduction

Aerial vehicle has attracted much attention in research communities in recent years [1, 2]. The aerial vehicle has high maneuverability as it can overcome the restriction from the terrain [3]. The research on motion planning and control of aerial vehicles has achieved great success [4–7]. In the past years, the aerial vehicle has been used to deal with various aerial tasks such as rescue and search [8, 9], exploration and mapping [10], and manipulation [11–14].

With the rapid growth of aerial vehicles, the requirements on the safety of the aerial vehicle especially for unmanned aerial vehicles are also growing. Fault-tolerant control is an important topic that should be considered to increase the safety of aerial vehicles. Because aerial vehicles are moving in air, the fault of the actuators of the aerial vehicle may induce serious results if there is no fault-tolerant control mechanism. Many researchers have investigated on this topic. The fault-tolerant control of aerial vehicles can mainly be divided into two groups of method.

One group is the active fault-tolerant control for the aerial vehicle. This methodology aims to detect and isolate the fault occurs on the actuators. Zhang et al. proposed a method using fault-tolerant control combined with trajectory replanning to revise the reference trajectory when actuator faults occur [15]. A fault-tolerant control for complete rotor failure is proposed in [16]. In [17], fault-tolerant control for tilted rotor hexacopter is presented; the idea of the algorithm is reconstructing the control allocation of the aerial robot with the help of tilted rotor. In [18], several fault detection and diagnosis (FDD) and fault-tolerant control (FTC) techniques are applied to unmanned quadrotor aerial vehicles. In [19], the emergency fault-tolerant controller for quadrotor UAVs suffering from a total loss of one actuator is considered. Experimental test of the Kalman filter-based fault-tolerant control is presented in [20]. Sadeghzadeh et al. also proposed a gain-scheduled PID control of aerial vehicles for the fault-tolerant control purpose [21]. A robust linear parameter varying observer is designed in order to detect the fault of the actuators of aerial vehicles in [22].

Avram et al. proposed a nonlinear estimator-based fault detection and isolation mechanism for quadrotor [23]. In [24], a Tau observer is used to design the fault diagnosis of quadrotor UAV. In [25], the active fault-tolerant control for sensor faults is also considered.

Another kind of methodology is the passive fault-tolerant control. This category of method usually relies on the adaptive control or learning-based control. Liu et al. proposed a fuzzy logic control method in order to deal with the actuator fault [26]. In [27], a nonlinear adaptive law is designed for the aerial vehicle in order to deal with the actuator effectiveness loss. Avram et al. also proposed a nonlinear adaptive fault-tolerant altitude and attitude tracking algorithm for quadrotor [28]. In their methods, there are no fault detection and isolation schemes. In [29], the fault-tolerant scheme based on adaptive control for the quadrotor at take-off phase is analyzed.

In general, the active fault-tolerant control is based on estimator or parameter identification. By comparing the estimated state to the sensed state, or comparing the estimated input with the desired input, the fault detection and isolation scheme can be designed. While the passive fault-tolerant control mechanisms are actually adaptive control laws which compensate the disturbance force and torque induced by the actuator faults. The active fault-tolerant control detects the fault actuators, so it is more flexible for control purpose. The detected and isolated fault can provide reference for planning and decision. Although it is believed that the fault detection and isolation mechanism influences the fastness of the fault-tolerant control, the existing research shows that the active fault-tolerant control can satisfy the requirement of stable control in most cases [23].

Normally, the input to the dynamics of underactuated aerial vehicles comprises thrust and three torques. In order to increase the load capacity of the aerial vehicle, redundant actuators are usually adopted, e.g., the hexarotor aircraft and the eight-rotor aircraft. When redundant actuators are used, the detection of the actuator fault becomes difficult, as the mapping between the actuators and the force/-torque is not one-to-one. This invites the problem of fault-tolerant control for underactuated aerial vehicles with redundant actuators.

Aiming to increase the safety of the underactuated aerial vehicles, in this paper, we deal with the fault-tolerant control problem for aerial vehicles with redundant actuators. We decide to adopt the active fault-tolerant control as we want to detect and isolate actuator fault. In order to let the vehicle be capable of recovering from arbitrary state error, a global control is adopted as the baseline controller. We use robust parameter identification method to estimate the force and torques. To deal with the problem induced by the redundant actuators, a fault isolation algorithm for the redundant actuators is proposed from mathematical analysis. The fault isolation algorithm compares every actuator so as to solve the actual actuator effect from the estimated force and torques. We will show the uniqueness and existence of the solution when there are redundant actuators under certain assumptions. The entire fault-tolerant mechanism is demonstrated in hexarotor and eight-rotor aircraft which are two kinds of typical underactuated aerial vehicles with redundant actuators.

This paper is composed of five sections. Section 2 formulates the problem of this paper. Fault detection and isolation mechanism for the redundant actuators is presented in Section 3. In Section 4, numerical simulation results for two typical aerial vehicles with redundant actuators are presented.

2. Problem Formulation

2.1. Dynamics of Underactuated Aerial Vehicles. In this paper we consider the underactuated aerial vehicle whose EOM (equation of motion) can be expressed as follows [30]:

$$\begin{aligned} \dot{p} &= v, \\ \dot{v} &= ge_3 - \frac{T}{m}\mathrm{Re}_3 - \frac{F\Delta}{m}, \\ \dot{R} &= R\widehat{\omega}, \\ \dot{\omega} &= M^{-1}(\tau - \tau_\Delta - \widehat{\omega}M\omega), \end{aligned} \tag{1}$$

where $p \in \mathbb{R}^3$ and $v \in \mathbb{R}^3$ are the position and velocity of the vehicle, $R \in SO$ (3) is the rotation matrix denoting the attitude of the aerial vehicle, $\omega \in \mathbb{R}^3$ is the angular velocity expressed in body frame, $m \in \mathbb{R}$ and $M \in \mathbb{R}^{3\times3}$ denote the mass and the inertia tensor of the vehicle, respectively, $T \in \mathbb{R}$ and $\tau \in \mathbb{R}^3$ are the net thrust and the body torque of the vehicle, $F_\Delta \in \mathbb{R}^3$ and $\tau_\Delta \in \mathbb{R}^3$ represent the disturbance force and torque, $e_3 = (0, 0, 1)^T$, g is the constant of acceleration due to gravity, and $\widehat{\omega}$ is the heat map of $\omega = (\omega_1, \omega_2, \omega_3)^T$:

$$\widehat{\omega} = \begin{bmatrix} 0 & -\omega_3 & \omega_2 \\ \omega_3 & 0 & -\omega_1 \\ -\omega_2 & \omega_1 & 0 \end{bmatrix}. \tag{2}$$

Note that the z axis of the inertial frame for (1) coincides with the gravity direction, and the definition of the body-fixed frame accords to front-right-down habit. The first and third equations in (1) are the kinematics part of the EOM, while the second and the fourth equations in (1) are the dynamics part of the EOM.

It is seen that the underactuated aerial vehicle has four control effects. As the thrust is in one direction, this type of aerial vehicle can increase the efficiency compared to the fully actuated aerial vehicles.

For underactuated aerial vehicle, the total thrust T and torque τ is generated by actuators. In this paper, we consider the linear relationship between the thrust/torque and the input of the actuators, as shown in the following expression:

$$\begin{bmatrix} \tau \\ T \end{bmatrix} = AW, \tag{3}$$

where $A \in \mathbb{R}^{4\times n}$ is the allocation matrix, $W \in \mathbb{R}^n$ is the effect of the actuators, and n is the number of actuators. We denote by $S_\tau := \{[\tau, T]\} \subset \mathbb{R}^4$ the torque space and denote by $S_W :=$

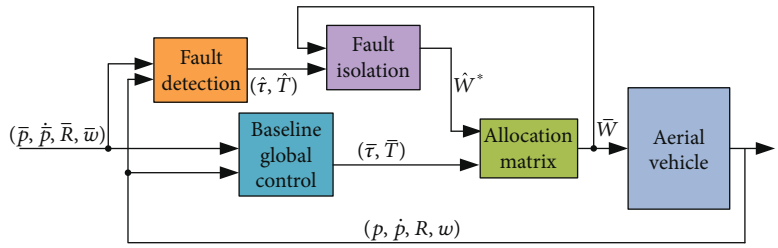

Figure 1: The overall scheme of the fault-tolerant control.

$\{W\} \subset \mathbb{R}^n$ the actuator space. Then, the allocation matrix induces a linear mapping $f_A : S_W \ni W \mapsto AW \in S_\tau$. If $n = 4$ and the rank of A is 4, then the mapping f_A is one-to-one. If $n > 4$, there exist the redundant actuators, and the mapping f_A is not one-to-one.

Assumption 1. The allocation matrix A is constant when there is no fault for the actuators.

Remark 1. From the EOM (1), one can design a baseline tracking controller for the aerial vehicle. In this paper, a global tracking controller for the aerial vehicle in [7] is adopted as the baseline controller. The global tracking controller ensures the global stability of the closed loop system, so it is more suitable to be used in fault-tolerant control. It generates the desired force/torque $(\bar{\tau}^T, \bar{T})^T$ and the desired actuator effect according to $\bar{W} = A^+(\bar{\tau}^T, \bar{T})^T$, where A^+ is the Moore-Penrose pseudoinverse of A. For brevity, the detailed design and analysis of the baseline controller is not introduced in this paper.

2.2. Definition of Fault. In this paper we consider the partial loss of effect of actuators. The effect of the faulty actuator is modeled as proportional to the desired actuator effect as

$$W_i = \alpha \bar{W}_i, \tag{4}$$

where W_i represents the actual effect of actuator i and $\bar{W}_i$ is the desired effect of actuator i. Under this definition, $\alpha = 1$ means no fault, while $\alpha = 0$ means complete fault. Note that due to the redundant actuators, different faults may induce the same force/torque which is the actual input of the dynamics of the aerial vehicle.

Under the definition of (4), when there is actuator fault, the torque and the net thrust generated by the actuators can be expressed as

$$\begin{bmatrix} \tau \\ T \end{bmatrix} A \Lambda_i \bar{W}, \tag{5}$$

where Λ_i is a diagonal matrix whose diagonal elements are all 1 except the i-th element is α_i.

Assumption 2. During the flight, fault occurs to only one of the actuators at one time.

Remark 2. The above assumption coincides with the actual applications. As in the real application cases, once there exists fault in the aerial vehicle, the corresponding decision can be made, e.g., to reconstruct the controller and to land the vehicle soon.

The overall scheme of the fault detection and isolation proposed in this paper is shown in Figure 1. Because we will use active fault-tolerant algorithm, the fault is detected and isolated when fault occurs. Once the fault on the redundant actuators is isolated, the allocation matrix will be reconstructed so as to generate the desired force and torque to guarantee the stability of the vehicle. We will let $\hat{W} = f_A^{-1}([\hat{\tau}, \hat{T}])$ denote the estimated actuator effect and let $\hat{W}^*$ denote the isolated actuator effect.

3. Fault Detection and Isolation considering Redundant Input

In this section, fault detection and isolation mechanism is designed. The purpose of the parameter identification is to detect the fault. The parameter identification algorithm identifies the force/torque $(\tau^T, T)^T$. Given that the aircraft has 4 independent degrees of freedom in the motion modeling, $(\tau^T, T)^T$ detected from the identification is unique. However, it should be noted that due to the redundant actuators, the identified force/torque may map to multiple possible solutions of actuator effect. Therefore, the fault needs to be further isolated. The fault isolation algorithm calculates the actuator effect according to the identified force/torque and desired actuator effect.

3.1. Fault Detection through Parameter Identification. In this paper we adopt the Hinf-based algorithm for the parameter identification in order to detect the fault of aerial vehicles. In order to adopt the parameter identification method, the force/torque $(\tau^T, T)^T$ is treated as the unknown parameters. Following [31–34], we rewrite the dynamics of the aerial vehicle into the following state-space form for the parameter identification purpose,

$$\begin{aligned} \dot{x} &= a(x)\chi + b(x) + d_p, \\ y &= x + d_m, \end{aligned} \tag{6}$$

where $\chi = (\tau^T, T)^T \in \mathbb{R}^4$ is treated as unknown parameters to be estimated, $x = (\omega^T, v^T)^T \in \mathbb{R}^6$ is the system state, $y \in \mathbb{R}^6$ is

the measured state, $d_p = \left(-\left(M^{-1}\tau_\Delta\right)^T, -F_\Delta^T/m\right)^T$ is the disturbance, d_m denotes the measurement noise, and from (1) we have

$$a(x) = \begin{bmatrix} M^{-1} & 0 \\ 0 & -\dfrac{1}{m}\,\mathrm{Re}_3 \end{bmatrix}, \qquad b(x) = \begin{bmatrix} -M^{-1}\widehat{\omega}M\omega \\ ge_3 \end{bmatrix}. \tag{7}$$

Note that in this equation, the kinematics part of (1) is not included.

In this paper we assume that no prior knowledge of the actuator fault (occurrence time, magnitude, etc.) is available. We adopt the time-varying case of the Hinf-based parameter identification algorithm. Following [31, 33], we consider an assumed form of the parameter χ varying with time as

$$\dot{\chi}(t) = Kd_\chi, \qquad \chi|t_{=0} = \chi_0, \tag{8}$$

where $K \in \mathbb{R}^{4\times s}$ is the weighting matrix and $d_\chi \in \mathbb{R}^s$ indicates the bias/uncertainties. For the system defined in (6) and (8), the Hinf-based algorithm yields a guaranteed parameter identification error as

$$\frac{\|\chi - \widehat{\chi}\|_Q^2}{\|d_p\|_I^2 + \|d_m\|_I^2 + \|d_\chi\|_I^2 + |x_0 - \widehat{x}_0|_{P_0}^2 + |\chi - \widehat{\chi}_0|_{Q_0}^2} \le \gamma^2, \tag{9}$$

where $\widehat{\chi}_0 \in \mathbb{R}^4$ and $\widehat{x}_0 \in \mathbb{R}^6$ are the initial estimates of χ and x, and we specify both as the trimmed value for the steady hovering flight. The form $\|*\|_Q$ is an L_2 norm with a predefined semipositive weighting function $Q \ge 0$, and $\|*\|_Q$ is a generalized Euclidean norm $x^T Q_0 x$ with positive weight $Q_0 > 0$; both $P_0 \in \mathbb{R}^{6\times 6}$ and $Q_0 \in \mathbb{R}^{4\times 4}$ are determined by the user. Generally, (9) provides a guaranteed worst-case performance of the identification algorithm bounded by γ for any χ_0, x_0, and the uncertainties (d_p, d_m, and d_χ), so long as γ is larger than the minimum achievable disturbance attenuation level γ^*.

The time-varying case of the Hinf-based parameter identification algorithm is written as:

$$\begin{bmatrix} \dot{\widehat{x}} \\ \dot{\widehat{\chi}} \end{bmatrix} = \begin{bmatrix} 0 & a(y) \\ 0 & 0 \end{bmatrix} \begin{bmatrix} \widehat{x} \\ \widehat{\chi} \end{bmatrix} + \begin{bmatrix} b(y) \\ 0 \end{bmatrix} + \sum^{-1} \begin{bmatrix} I \\ 0 \end{bmatrix} (y - \widehat{x}), \tag{10}$$

where $\Sigma = \Sigma(t) \in \mathbb{R}^{10\times 10}$ is defined as

$$\dot{\sum} = -\sum \begin{bmatrix} 0 & a(y) \\ 0 & 0 \end{bmatrix} - \begin{bmatrix} 0 & 0 \\ a(y)^T & 0 \end{bmatrix} \sum + \begin{bmatrix} I & 0 \\ 0 & -\gamma^{-2}Q \end{bmatrix} - \sum \begin{bmatrix} I & 0 \\ 0 & KK^T \end{bmatrix} \sum, \tag{11}$$

with initial condition $\Sigma(0) = \mathrm{diag}\,(P_0, Q_0)$. Note that in (10) and (11), the dependency of $a(y)$ and $b(y)$ differs from (6), as we have the d_m corrupted measured state only.

One critical issue of the Hinf identification algorithm is to determine the minimum disturbance attenuation level γ^*. The time-invariant case has been discussed in [31, 32], and in [33], a general result was proved for the time-varying case. Here we adopt the conclusion directly as, by using the partition

$$\sum = \begin{bmatrix} \sum_1 & \sum_2 \\ \sum_2^T & \sum_3 \end{bmatrix}. \tag{12}$$

With $\Sigma_1 \in \mathbb{R}^{6\times 6}$, $\gamma^* = 1$ can be achieved by specifying $P_0 = I$ and $Q = \sum_2^T \sum_1^{-2} \sum_2$ for any $Q_0 > 0$.

It should be noticed that in order to adopt (10) to identify $(\tau^T, T)^T$, we need the knowledge of the parameters of the vehicles, i.e., the inertial parameters, the mass, and the parameters in the allocation matrix, etc. It is assumed that these parameters are identified *a prior* already.

3.2. Fault Isolation with Redundant Actuators

3.2.1. Solution Uniqueness and Existence

Assumption 3. The number of the aerial vehicle's actuators is more than or equal to 6.

Assumption 4. The mapping $f_A : S_W \ni W \mapsto AW \in S_\tau$ is surjective, i.e., for every $(\tau^T, T)^T \in S_\tau$, there exists at least one $W \in S_W$ with $f_A(W) = (\tau^T, T)^T$.

Assumption 5. For every $(\widehat{\tau}^T, \widehat{T})^T \in S_\tau$,

$$\mathrm{rank}\,(A) = \mathrm{rank}\left(\left[A \,\middle|\, \begin{matrix} \widehat{\tau} \\ \widehat{T} \end{matrix}\right]\right) = 4, \tag{13}$$

where rank $(*)$ denotes the rank of matrix $*$. Moreover, any submatrix of A composed of arbitrary 2 columns of A is full column rank, we write it as,

$$\mathrm{rank}\,(A_{\mathrm{sub}}) = 2. \tag{14}$$

For every $(\widehat{\tau}^T, \widehat{T})^T \in S_\tau$, consider the following linear equation with unknown variable $W \in \mathbb{R}^n$

$$AW = \begin{bmatrix} \widehat{\tau} \\ \widehat{T} \end{bmatrix}, \tag{15}$$

when (13) is satisfied and $n \geq 6$, (15) has multiple solutions. Therefore, from Assumption 3–5, we can conclude that for $(\widehat{\tau}^T, \widehat{T})^T \in S_\tau$, there may be *multiple* $\widehat{W} \in S_W$ s.t. $f_A(\widehat{W}) = (\widehat{\tau}^T, \widehat{T})^T$. Thus, we cannot directly use (4) to calculate the fault factors from $(\widehat{\tau}^T, \widehat{T})^T$. In order to calculate the fault factors, we need to isolate the actuator effect. The following theorem gives the result that isolating the unique solution of actuator effect from $(\widehat{\tau}^T, \widehat{T})^T$ and $\bar{W}$ is feasible.

Theorem 1. *Under Assumptions 1–5, given every* $(\widehat{\tau}^T, \widehat{T})^T \in S_\tau$, *if the identification error is 0, one can solve the actual actuator effect* $\widehat{W}^* \in S_W$ *from* $(\widehat{\tau}^T, \widehat{T})^T$ *and* $\bar{W}$, *the solution* $\widehat{W}^*$ *exists and is unique.*

Proof 1. In order to isolate the actual faulty actuator from the identified force and torque, we have to solve the linear equation (15) with unknown actuator effect $W \in \mathbb{R}^n$. As discussed before, if the actuator allocation is redundant, the actuator effect solution of (15) is multiple, and the isolated actuator effect is one of the multiple solutions of (15).

It is obvious that one solution of (15) is

$$\widehat{W} = A^+ \begin{bmatrix} \widehat{\tau} \\ \widehat{T} \end{bmatrix}. \tag{16}$$

In order to isolate fault, let us consider the null space of the allocation matrix: $\text{Null}(A) \subset \mathbb{R}^n$. If $W \in S_W$, $\iota \in \text{Null}(A)$, and $f_A(W) = (\tau^T, T)^T$, then we have $f_A(W + \iota) = (\tau^T, T)^T$.

We define the following matrix composed from the basis vectors of $\text{Null}(A)$ as

$$N = [a_1, a_2, a_3, \ldots, a_n - 4], \tag{17}$$

where $a_i \in \mathbb{R}^n$ is the basis vector of $\text{Null}(A)$. For any $\nu \in \mathbb{R}^{n-4}$, we have $N\nu \in \text{Null}(A)$.

From (14) in Assumption 5, it can be seen that any submatrix of N composed of arbitrary $n-2$ rows of N is full column rank (see Appendix). We write it as

$$\text{rank}\,(N_{\text{sub}}) = n - 4. \tag{18}$$

As the identification error of $(\tau^T, T)^T$ is 0, the solution for the following equation exists and is unique if there is fault in actuator i.

$$\widehat{W} + N\nu = \Lambda_i \bar{W}, \tag{19}$$

where $\nu \in \mathbb{R}^{n-4}$ is the unknown variable to be solved. Let ν^* denote the solution of (19), we have $\widehat{W} + N\nu^* \in S_W$.

Since the solution of the linear equation (19) exists and is unique, we have

$$\text{rank}\,(N) = \text{rank}\left(\left[N \middle| \Lambda_i \bar{W} - \widehat{W}\right]\right) = n - 4. \tag{20}$$

The purpose of the isolation is to obtain the actual actuator effect by finding out the location of the fault and then solving (19). Given the location of the actuator fault, it is seen that solving (19) is tractable. Then, the key problem is how to find out the location of the fault. Later, we will show that (19) is solvable only for the faulty actuator. From this property, we will isolate the location of the fault by comparing all of the equations corresponding to all of the actuators.

Now, we consider if it is possible to conclude from $\widehat{W}$ and $\bar{W}$ that another actuator fault j took place. That is, consider the existence of solution for the following equation with unknown variable $\nu \in \mathbb{R}^{n-4}$.

$$\widehat{W} + N\nu = \Lambda_j \bar{W}, \quad j \neq i. \tag{21}$$

Now, proof of this theorem becomes proof that (21) is not solvable. We will prove it by reduction to absurdity.

We assume (21) is solvable, then we have

$$\text{rank}\,(N) = \text{rank}\left(\left[N \middle| \Lambda_j \bar{W} - \widehat{W}\right]\right) = n - 4, \tag{22}$$

which means the solution of (21) is also unique.

Removing the i-th and j-th components, the remaining parts of (19) and (21) are the same. We write the shared part of (19) and (21) as

$$\widehat{W}_{i,\bar{j}} + N_{i,\bar{j}}\nu = \bar{W}_{i,\bar{j}}, \tag{23}$$

which is solvable. Moreover, from (18), it is seen

$$\text{rank}\left(N_{i,\bar{j}}\right) = n - 4. \tag{24}$$

Then, the solution of (23) is also unique.

Notice that the solution of (19) is also the solution of (23), and the solution of (21) is also the solution of (23). As the solutions of (23), (19), and (21) are all unique, we can conclude the solutions of (19) and (21) are the same.

Substituting the solution ν^* into (19) and (21) and selecting the j-th component of (19) and (21), we have

$$\begin{aligned} \widehat{W}_j + N_j\nu^* &= \bar{W}_j, \\ \widehat{W}_j + N_j\nu^* &= \alpha_j \bar{W} j, \end{aligned} \tag{25}$$

which is contradictory as $\alpha_j \neq 1$. Therefore, we can conclude that the assumption that (21) is solvable is not correct.

In summary, if a fault occurs at actuator i, for unknown variable $\nu \in \mathbb{R}^{n-4}$,

$$\widehat{W} + N\nu = \Lambda_j \bar{W} \text{ is} \begin{cases} \text{solvable}, & j = i, \\ \text{unsolvable}, & j \neq i. \end{cases} \tag{26}$$

Fault isolation algorithm
Fault Isolation Algorithm
$i = 1$;
min_norm = inf ;
while (*i*<=*n*)
{ $\begin{bmatrix} v^* \\ 1 - a_i^* \end{bmatrix} = [N \quad \Gamma_i]^+ (\bar{W} - \hat{W})$;
norm = $\left\| [N \quad \Gamma_i] \begin{bmatrix} v^* \\ 1 - a_i^* \end{bmatrix} - (\bar{W} - \hat{W}) \right\|$;
if (min_norm >=norm)
{ min_norm >=norm;
$\hat{v}^* = v^*$;
$i_f = i$;
}
$i = i + 1$;
}

Algorithm 1

From this property, we can therefore find actuator i by comparing the n equations and obtain the solution v^*. The actual actuator effect is then given by

$$\hat{W}^* = \hat{W} + Nv^* \in S_W. \tag{27}$$

This completes the proof.

Remark 3. Theorem 1 indicates that when the identification error of $(\tau^T, T)^T$ is 0, we can always solve W from $\bar{W}$ and $(\hat{\tau}^T, \hat{T})^T$ uniquely. However, as the identification error always exists due to the disturbances and noises in the system, (19) may be unsolvable. In this case, we modify (19) to let it be solvable.

$$\hat{W} + Nv = \Lambda_i \bar{W} + \Delta W, \tag{28}$$

where ΔW is determined by the identification error of $(\tau^T, T)^T$. Then, it can still be proved that $\hat{W} + Nv = \Lambda_j \bar{W} + \Delta W$ is not solvable for any $j \neq i$. The proof is similar to the proof of Theorem 1.

3.2.2. Fault Isolation Algorithm. If we consider the identification error, from Remark 3, it is seen that one needs to solve (28) in order to isolate the actual fault actuators. However, as the identification error of $(\tau^T, T)^T$ is not possible to be accurately obtained, ΔW cannot be obtained accurately. In order to overcome this problem, we propose a fault isolation algorithm by comparing the different actuators.

For the n actuators, we can write n equations with each similar to (19),

$$[N \quad \Gamma_i] \begin{bmatrix} v \\ 1 - a_i \end{bmatrix} = \bar{W} - \hat{W}, \quad i = 1, 2, \ldots, n, \tag{29}$$

where $v \in \mathbb{R}^{n-4}$ and $\alpha_i \in \mathbb{R}$ are unknown variables, $\Gamma_i \in \mathbb{R}^{n \times 1}$ is a vector whose i-th element is $\bar{W}_i$ and other elements are 0. Notice that when there is identification error, there may be no solutions for all the n equations in (29). Therefore, we adopt least-squares solution of (29) as

$$\begin{bmatrix} v^* \\ 1 - a_i^* \end{bmatrix} = [N \quad \Gamma_i]^+ \left(\bar{W} - \hat{W}\right), \quad i = 1, 2, \ldots, n. \tag{30}$$

We select the faulty rotor i_f by comparing the n equations' solutions,

$$i_f = \underset{i = 1, 2, \ldots, n}{\operatorname{argmin}} \left\| [N \quad \Gamma_i] \begin{bmatrix} v^* \\ 1 - a_i^* \end{bmatrix} - \left(\bar{W} - \hat{W}\right) \right\|, \tag{31}$$

The corresponding least-squares solution for i_f-th equation is

$$\begin{bmatrix} v^* \\ 1 - \hat{a}_i^* \end{bmatrix} = \left[N \quad \Gamma_{i_f} \right]^+ \left(\bar{W} - \hat{W}\right). \tag{32}$$

Then, the isolated actuator effect is

$$\hat{W}^* = \hat{W} + N\hat{v}^*. \tag{33}$$

And the fault factor $\hat{\Lambda}$ is calculated from $\hat{W}^* = \hat{\Lambda} \bar{W}$.

The algorithm for the fault isolation is summarized in Algorithm 1. Because the number of the actuator is always finite, the computational complexity of this algorithm is light. Therefore, the algorithm can be run in real time.

Remark 4. Once the fault of the actuator is isolated, the allocation matrix should be reconstructed using the isolated fault factor as

$$\hat{A} = A\hat{\Lambda}. \tag{34}$$

Remark 5. If there is another fault after a fault has occurred, then the new fault can also be identified and isolated using the methodology introduced in this paper. In order to isolate the new fault, the reconstructed allocation matrix should satisfy Assumption 3–5.

4. Application Results

In this section, the proposed fault-tolerant control will be applied to hexarotor aircraft and eight-rotor aircraft to demonstrate its effectiveness. The numerical simulation is finished in MATLAB/Simulink. EOM (1) is adopted as the plant model in the simulation.

4.1. Case 1: Fault-Tolerant Control of Hexarotor. The typical configuration of the hexarotor is shown in Figure 2. Because the six rotors are parallel, the allocation matrix of hexarotor satisfies Assumption 3–5.

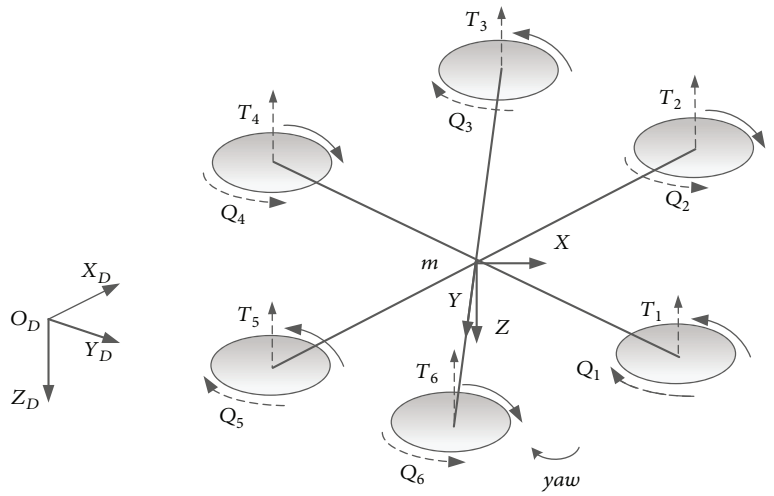

Figure 2: Configuration of hexarotor.

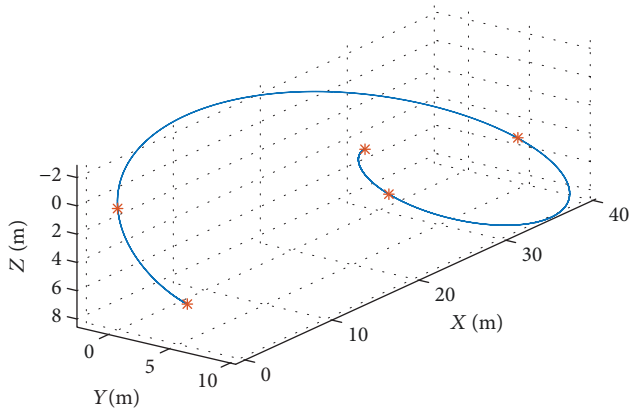

Figure 3: The minimal snap reference trajectory, case 1.

Following the coordinate frame definition in Figure 2, the allocation matrix of the hexarotor is obtained as

$$A = \begin{bmatrix} -\frac{1}{4}d_r & \frac{1}{4}d_r & \frac{1}{2}d_r & \frac{1}{4}d_r & -\frac{1}{4}d_r & -\frac{1}{2}d_r \\ \frac{\sqrt{3}}{4}d_r & \frac{\sqrt{3}}{4}d_r & 0 & -\frac{\sqrt{3}}{4}d_r & -\frac{\sqrt{3}}{4}d_r & 0 \\ \frac{k_d}{k_t} & -\frac{k_d}{k_t} & \frac{k_d}{k_t} & -\frac{k_d}{k_t} & \frac{k_d}{k_t} & -\frac{k_d}{k_t} \\ 1 & 1 & 1 & 1 & 1 & 1 \end{bmatrix} k_t, \quad (35)$$

where k_t is the thrust coefficient of each rotor, k_d is drag coefficient of each rotor, and d_r is the distance between the diagonal pair of rotors.

The reference trajectory in this case is a minimum snap trajectory connecting five points [35], as shown in Figure 3. The five set points are (20,6,0.2), (20,8,3), (39,5,5), (0,0,0), and (1,5,6) m. In the simulation, the parameters of the aerial vehicle are $M = \text{diag}([0.226249; 0.224466; 0.354769])\text{kg}\cdot\text{m}^2$, $m = 6.05$ kg. These parameters are from parameters of

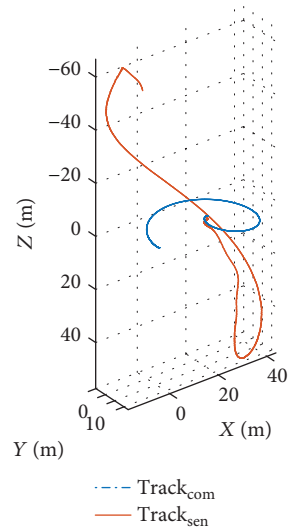

(a) The 3D-tracking of the hexarotor without fault-tolerant control, case 1

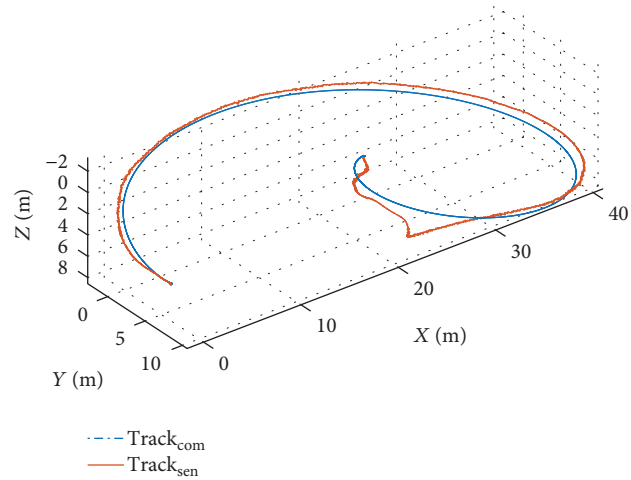

(b) The 3D-tracking of the hexarotor using fault-tolerant control, case 1

Figure 4: The 3-D position profile of the hexarotor, case 1.

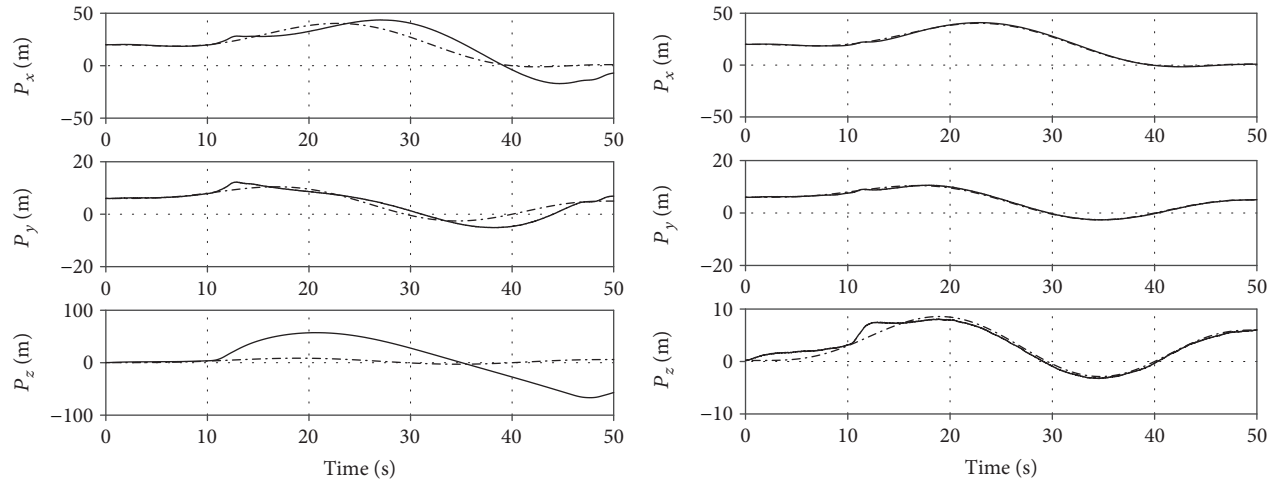

(a) The position profile of the hexarotor without fault-tolerant control, case 1

(b) The position profile of the hexarotor using fault-tolerant control presented in this paper, case 1

Figure 5: The position profile of the hexarotor, case 1.

the DJI S900. In order to increase the fidelity of the simulation, sensor noise and delays are added in the feedback. The delay in the angular velocity and attitude feedback loop is 0.02 s, while the delay in the velocity and position feedback loop is 0.1 s. The variance of the noise added in the feedback is 0.001 rad/s, 0.01, 0.02 m/s, and 0.1 m for the angular velocity, rotation matrix, velocity, and position loop, respectively. The parameter uncertainty is also considered in the simulation. The inertial parameters, the mass, and the actuator parameters of the vehicle used in the controller are set to be 0.8 times as the parameters in dynamics. The rotational speed of each rotor is restricted in the range of $[0, 625]$rad/s, which is equal to $[0, 5971]r/\text{min}$. The motor-propeller actuator is modeled as a second-order system whose frequency and bandwidth are 1.414 and 30, respectively. In the numerical simulation, we also need to specify Q_0 and K. Following [34], we set $Q_0 = 3 \times 10^{-7} I_4$ and $KK^T = 10 I_4$ for all the simulation cases in this paper.

In this simulation case, the fault is injected to rotor-1 at 10 s. The fault factor is set to $\alpha = 0.3$. The proposed fault-tolerant control mechanism begins to work at 5 s. During the run, because of the existence of noise and uncertainties, there may exist fault factor greater than 1 or less than 0, which should be omitted in the run.

The results are shown in Figures 4–6. The reference and response trajectory of the vehicle without using the fault-tolerant control is shown in Figures 4(a) and 5(a). And the corresponding profile of the vehicle using the fault-tolerant control scheme is shown in Figures 4(b) and 5(b). It is seen the vehicle cannot be stabilized when the fault occurs in the case no fault-tolerant control scheme is used. While in the case where fault-tolerant control scheme is used, the vehicle can stay stable in the presence of fault. The vehicle deviates a little from the reference trajectory, but the tracking error converges after the fault of the rotors is isolated and the controller is reconstructed. The isolated fault factor is shown in Figure 6. This is in line with the injected fault. From Figure 6, it is also seen that there is

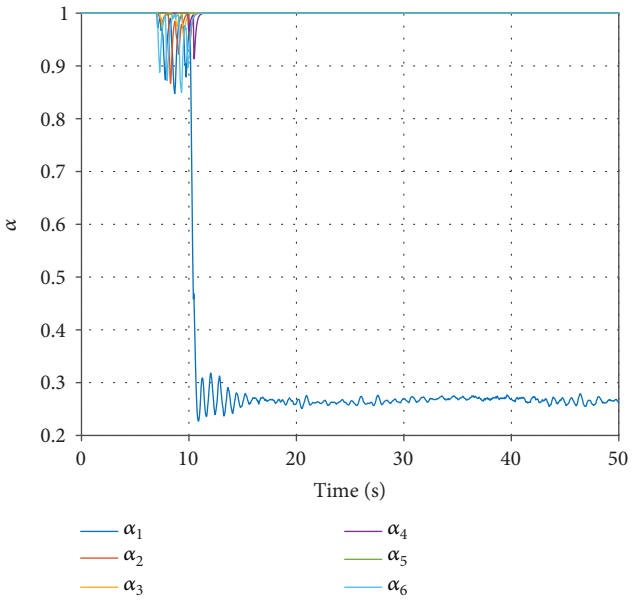

Figure 6: The isolated fault factor for the actuators, case 1.

estimation error, which is induced by the uncertainties, e.g., the inaccurate parameters, the actuator dynamics, and the measurement noise.

4.2. Case 2: Fault-Tolerant Control of Eight-Rotor Aircraft. In this case, the eight-rotor aircraft whose configuration shown as Figure 7 is considered. The allocation matrix of this kind of aircraft is expressed in (36).

In this simulation case, the fault is injected to rotor-1 at 14 s. The fault factor is set to $\alpha = 0.4$. The noise and uncertain parameters are also considered as in case 1. The speed of the rotors is also bounded into $[0, 625]rad/s$. The fault-tolerant scheme begins at 7 s.

The reference trajectory for the eight-rotor aircraft is a circle whose equation is $\bar{P} = (7.5 \cos((3/7.5)t), 7.5 \sin$

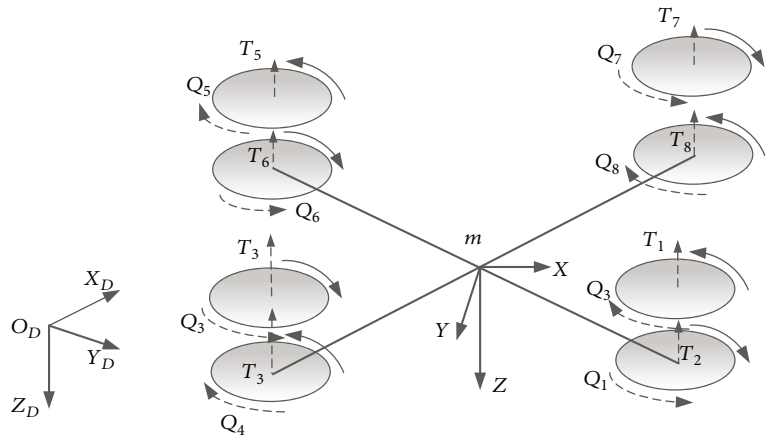

Figure 7: The configuration of eight-rotor aircraft.

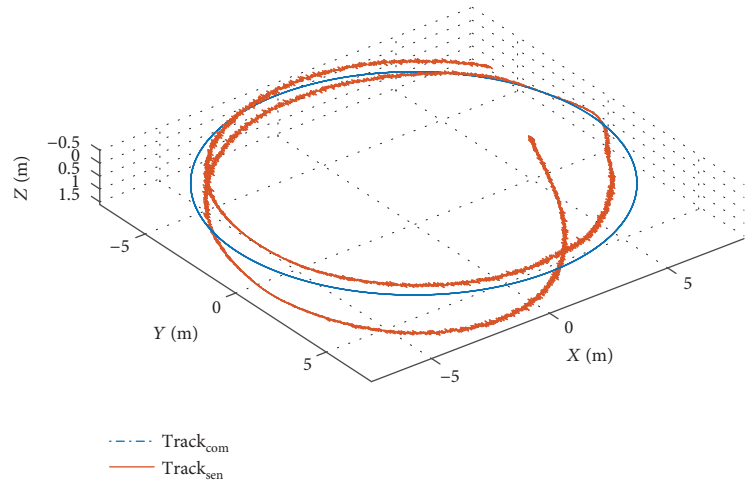

Figure 8: The reference trajectory and the response trajectory using the fault-tolerant control scheme, case 2.

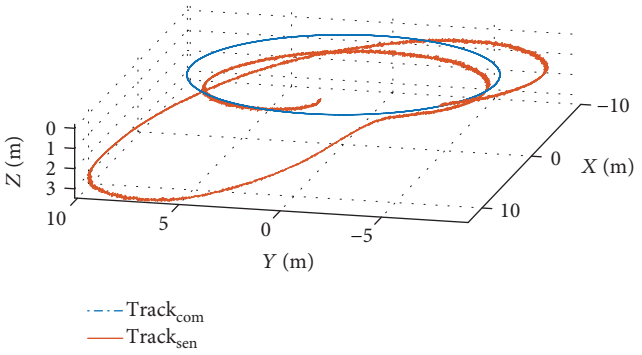

Figure 9: The reference trajectory and the response trajectory not using the fault-tolerant control scheme, case 2.

$((3/7.5)t), 0)^T$. The initial position of the vehicle is set to $(5, 0, 0)^T$, all in unit of m. The results are shown in Figures 8–11. The response trajectory using the proposed fault-tolerant control scheme is shown in Figure 8. As a comparison, the response trajectory without using the proposed fault-tolerant control mechanism is shown in Figure 9. It is shown the deviation of the response from the reference

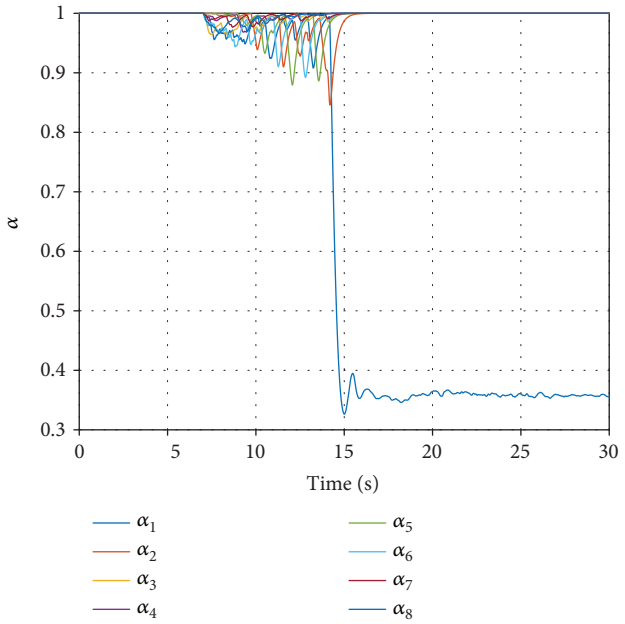

Figure 10: The isolated fault factors of the eight rotors, case 2.

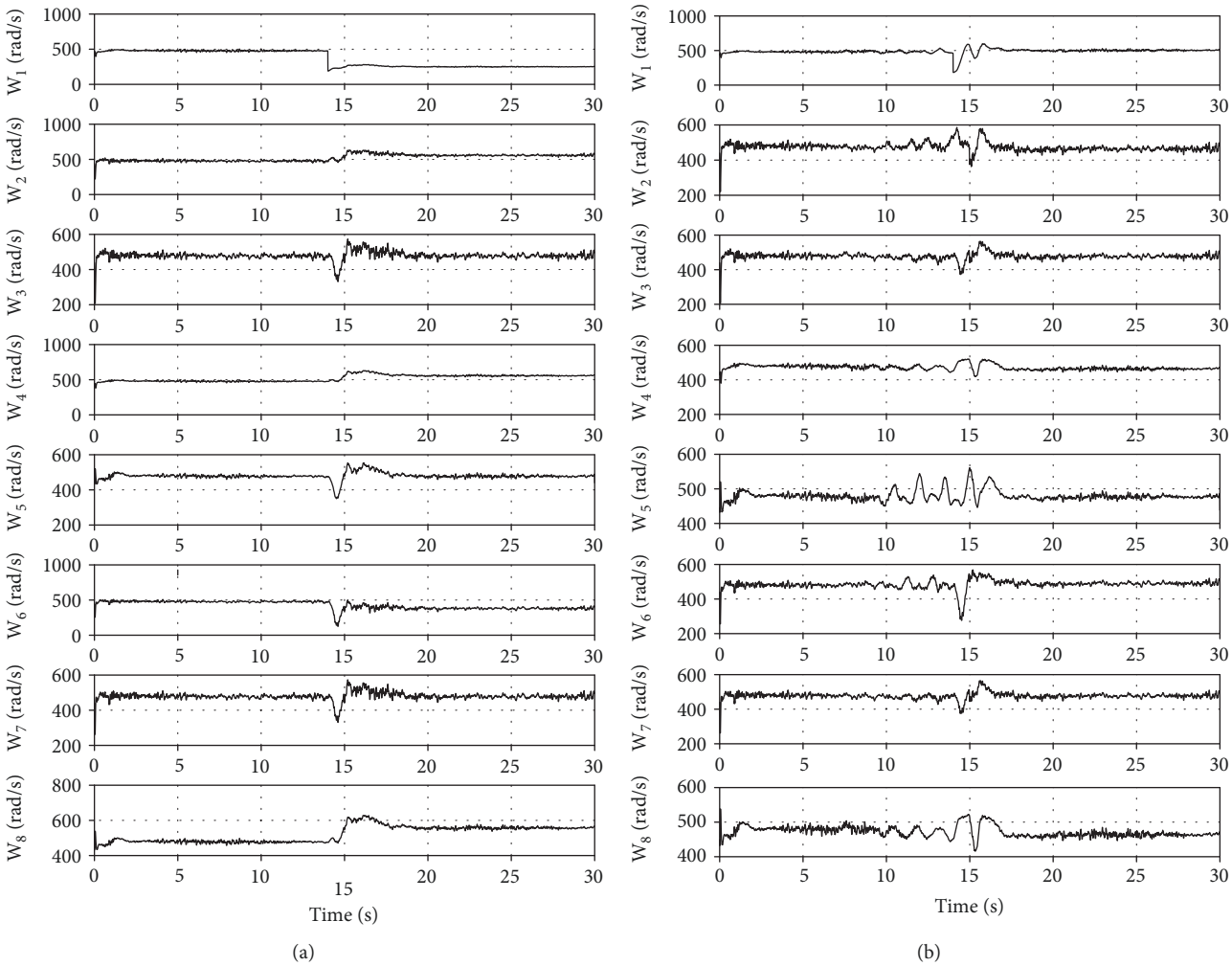

Figure 11: The actual rotor speed under fault-tolerant control (a) and the actual rotor speed without using the fault-tolerant control mechanism (b), case 2.

trajectory is bigger when the fault-tolerant control mechanism is not used. The isolated fault factor is plotted in Figure 10. It is seen the fault is detected and isolated using the scheme proposed in this paper. Furthermore, the actual rotational speed of the eight rotors is shown in Figure 11. It is seen that the baseline controller itself can stabilize the vehicle when the fault occurs. However, from the right part of Figure 11, it is seen the result is that the rotor speed varies obviously before and after the occurrence of the fault. And from the left part of Figure 11, it is seen the rotor speed does not vary greatly after the fault occurs because of the regulation of the fault-tolerant scheme. Therefore, the proposed mechanism can keep the effect of the actuators. This is valuable for keeping the actuators work in normal conditions.

5. Conclusions

In the active fault-tolerant isolation and control mechanism presented in this paper, a robust parameter identification method has been designed as the fault detection algorithm. We have also analyzed and designed the fault isolation

$$A = \begin{bmatrix} -\frac{\sqrt{2}}{4}d_r k_t & -\frac{\sqrt{2}}{4}d_r k_t & -\frac{\sqrt{2}}{4}d_r k_t & -\frac{\sqrt{2}}{4}d_r k_t & \frac{\sqrt{2}}{4}d_r k_t & \frac{\sqrt{2}}{4}d_r k_t & \frac{\sqrt{2}}{4}d_r k_t & \frac{\sqrt{2}}{4}d_r k_t \\ \frac{\sqrt{2}}{4}d_r k_t & \frac{\sqrt{2}}{4}d_r k_t & -\frac{\sqrt{2}}{4}d_r k_t & -\frac{\sqrt{2}}{4}d_r k_t & -\frac{\sqrt{2}}{4}d_r k_t & -\frac{\sqrt{2}}{4}d_r k_t & \frac{\sqrt{2}}{4}d_r k_t & \frac{\sqrt{2}}{4}d_r k_t \\ k_d & -k_d & k_d & -k_d & k_d & -k_d & k_d & -k_d \\ k_t & k_t & k_t & k_t & k_t & k_t & k_t & k_t \end{bmatrix} \quad (36)$$

mechanism considering the redundant actuators. The theoretical results have been obtained through mathematical proof. Practical isolation algorithm has also been proposed in order to deal with the uncertainties in systems. Several numerical simulation cases have been conducted in order to verify the proposed algorithm. The proposed fault-tolerant control method is valuable for increasing the safety of the underactuated aerial vehicle with redundant actuators. By using the proposed algorithm, the fault actuators can be detected and isolated. This is the basis for reconstruction of flight controller and provides foundation for the decision making. In future works, the high level motion planning method for the fault-tolerant purpose will be considered.

Appendix

If there exists N_{sub}s.t.rank$(N_{\text{sub}}) < n-4$, one can always write N into the following format by applying column operations and row switchings to N,

$$N = \begin{bmatrix} N_{11} & N_{12} \\ N_{21} & 0_{(n-2)\times 1} \end{bmatrix}, \tag{A.1}$$

where $N_{11} \in \mathbb{R}^{2\times(n-5)}$, $N_{12} \in \mathbb{R}^{2\times 1}$, and $N_{21} \in \mathbb{R}^{(n-2)\times(n-5)}$. Then switching the corresponding columns of A, we transform A to $[A_1 \mid A_2]$, where $A_1 \in \mathbb{R}^{4\times 2}$, $A_2 \in \mathbb{R}^{4\times(n-2)}$, A_1 and A_2 satisfy

$$[A_1N_{11}|A_1N_{12}] + A_2\left[N_{21}\middle|0_{(n-2)\times 1}\right] = 0. \tag{A.2}$$

Then we have

$$A_1N_{12} = 0, \tag{A.3}$$

which leads to $N_{12} = 0$ because rank $(A_1) = 2$ (Assumption 5). This is contradictory to rank $(N) = n-4$. Therefore, rank $(N_{\text{sub}}) = n-4$ always satisfies.

Data Availability

The data used to support the findings of this study are available from the corresponding author upon request.

Conflicts of Interest

The authors declare that there is no conflict of interest regarding the publication of this paper.

Acknowledgments

This work was supported by the National Natural Science Foundation of China under Grant no. 51505014 and by the University of Michigan. The received funding did not lead to any conflict of interests.

References

[1] A. Tayebi and S. McGilvray, "Attitude stabilization of a VTOL quadrotor aircraft," *IEEE Transactions on Control Systems Technology*, vol. 14, no. 3, pp. 562–571, 2006.

[2] R. Mahony, V. Kumar, and P. Corke, "Multirotor aerial vehicles: modeling, estimation, and control of quadrotor," *IEEE Robotics and Automation Magazine*, vol. 19, no. 3, pp. 20–32, 2012.

[3] Y. Yu and X. Ding, "On hybrid modeling and control of a multi-propeller multifunction aerial robot with flying-walking locomotion," *Autonomous Robots*, vol. 38, no. 3, pp. 225–242, 2015.

[4] Y.-C. Choi and H.-S. Ahn, "Nonlinear control of quadrotor for point tracking: actual implementation and experimental tests," *IEEE/ASME Transactions on Mechatronics*, vol. 20, no. 3, pp. 1179–1192, 2015.

[5] Y. Yu, X. Ding, and J. J. Zhu, "Attitude tracking control of a quadrotor UAV in the exponential coordinates," *Journal of the Franklin Institute*, vol. 350, no. 8, pp. 2044–2068, 2013.

[6] Y. Yu and X. Ding, "A quadrotor test bench for six degree of freedom flight," *Journal of Intelligent and Robotic Systems*, vol. 68, no. 3-4, pp. 323–338, 2012.

[7] Y. Yu and X. Ding, "A global tracking controller for underactuated aerial vehicles: design, analysis, and experimental tests on quadrotor," *IEEE/ASME Transactions on Mechatronics*, vol. 21, no. 5, pp. 2499–2511, 2016.

[8] J. Roberts, D. Frousheger, B. Williams, D. Campbell, and R. Walker, "How the outback challenge was won: the motivation for the UAV challenge outback rescue, the competition mission, and a summary of the six events," *IEEE Robotics & Automation Magazine*, vol. 23, no. 4, pp. 54–62, 2016.

[9] J. Park, Y. Kim, and S. Kim, "Landing site searching and selection algorithm development using vision system and its application to quadrotor," *IEEE Transactions on Control Systems Technology*, vol. 23, no. 2, pp. 488–503, 2015.

[10] F. Fraundorfer, L. Heng, D. Honegger et al., "Vision-based autonomous mapping and exploration using a quadrotor MAV," in *2012 IEEE/RSJ International Conference on Intelligent Robots and Systems*, pp. 4557–4564, Vilamoura, Portugal, October 2012.

[11] A. Jimenez-Cano, G. H. J. Martin, A. Ollero, and R. Cano, "Control of an aerial robot with multi-link arm for assembly tasks," in *2013 IEEE International Conference on Robotics and Automation*, pp. 4916–4921, Karlsruhe, Germany, May 2013.

[12] X. Ding and Y. Yu, "Motion planning and stabilization control of a multipropeller multifunction aerial robot," *IEEE/ASME Transactions on Mechatronics*, vol. 18, no. 2, pp. 645–656, 2013.

[13] Y. Yu, X. Ding, and J. J. Zhu, "Dynamic modeling and control for aerial arm-operating of a multi-propeller multifunction aerial robot," *Advanced Robotics*, vol. 31, no. 13, pp. 665–679, 2017.

[14] Y. Yu and X. Ding, "Trajectory linearization control on so(3) with application to aerial manipulation," *Journal of the Franklin Institute*, vol. 355, no. 15, pp. 7072–7097, 2018.

[15] A. Chamseddine, Y. Zhang, C. A. Rabbath, C. Join, and D. Theilliol, "Flatness-based trajectory planning/replanning for a quadrotor unmanned aerial vehicle," *IEEE Transactions on Aerospace and Electronic Systems*, vol. 48, no. 4, pp. 2832–2848, 2012.

[16] P. Lu and E.-J. van Kampen, "Active fault-tolerant control for quadrotors subjected to a complete rotor failure," in *2015 IEEE/RSJ International Conference on Intelligent Robots and Systems (IROS)*, pp. 4698–4703, Hamburg, Germany, September-October 2015.

[17] J. I. Giribet, R. S. Sanchez-Pena, and A. S. Ghersin, "Analysis and design of a tilted rotor hexacopter for fault tolerance," *IEEE Transactions on Aerospace and Electronic Systems*, vol. 52, no. 4, pp. 1555–1567, 2016.

[18] Y. M. Zhang, A. Chamseddine, C. A. Rabbath et al., "Development of advanced FDD and FTC techniques with application to an unmanned quadrotor helicopter testbed," *Journal of the Franklin Institute*, vol. 350, no. 9, pp. 2396–2422, 2013.

[19] A. R. Merheb, H. Noura, and F. Bateman, "Emergency control of AR drone quadrotor UAV suffering a total loss of one rotor," *IEEE/ASME Transactions on Mechatronics*, vol. 22, no. 2, pp. 961–971, 2017.

[20] M. H. Amoozgar, A. Chamseddine, and Y. Zhang, "Experimental test of a two-stage kalman filter for actuator fault detection and diagnosis of an unmanned quadrotor helicopter," *Journal of Intelligent & Robotic Systems*, vol. 70, no. 1-4, pp. 107–117, 2013.

[21] I. Sadeghzadeh, A. Mehta, and Y. Zhang, "Fault/damage tolerant control of a quadrotor helicopter UAV using model reference adaptive control and gain-scheduled PID," in *AIAA Guidance, Navigation, and Control Conference*, pp. 1–13, Portland, Oregon, August 2011.

[22] F. R. López-Estrada, J.-C. Ponsart, D. Theilliol, Y. Zhang, and C.-M. Astorga-Zaragoza, "LPV model-based tracking control and robust sensor fault diagnosis for a quadrotor UAV," *Journal of Intelligent & Robotic Systems*, vol. 84, no. 1-4, pp. 163–177, 2016.

[23] R. C. Avram, X. Zhang, and J. Muse, "Quadrotor actuator fault diagnosis and accommodation using nonlinear adaptive estimators," *IEEE Transactions on Control Systems Technology*, vol. 25, no. 6, pp. 2219–2226, 2017.

[24] Z. Cen, H. Noura, T. B. Susilo, and Y. A. Younes, "Robust fault diagnosis for quadrotor UAVs using adaptive thau observer," *Journal of Intelligent & Robotic Systems*, vol. 73, no. 1-4, pp. 573–588, 2014.

[25] L. Qin, X. He, R. Yan, and D. Zhou, "Active fault-tolerant control for a quadrotor with sensor faults," *Journal of Intelligent & Robotic Systems*, vol. 88, no. 2–4, pp. 449–467, 2017.

[26] Z. Liu, C. Yuan, Y. Zhang, and J. Luo, "A learning-based fault tolerant tracking control of an unmanned quadrotor helicopter," *Journal of Intelligent and Robotic Systems*, vol. 84, no. 1–4, pp. 145–162, 2016.

[27] F. Chen, W. Lei, K. Zhang, G. Tao, and B. Jiang, "A novel nonlinear resilient control for a quadrotor UAV via backstepping control and nonlinear disturbance observer," *Nonlinear Dynamics*, vol. 85, no. 2, pp. 1281–1295, 2016.

[28] R. C. Avram, X. Zhang, and J. Muse, "Nonlinear adaptive fault-tolerant quadrotor altitude and attitude tracking with multiple actuator faults," *IEEE Transactions on Control Systems Technology*, vol. 26, no. 2, pp. 701–707, 2018.

[29] F. Chen, R. Jiang, K. Zhang, B. Jiang, and G. Tao, "Robust backstepping sliding-mode control and observer-based fault estimation for a quadrotor UAV," *IEEE Transactions on Industrial Electronics*, vol. 63, no. 8, pp. 1–5056, 2016.

[30] M.-D. Hua, T. Hamel, P. Morin, and C. Samson, "Introduction to feedback control of underactuated VTOLvehicles: a review of basic control design ideas and principles," *IEEE Control Systems Magazine*, vol. 33, no. 1, pp. 61–75, 2013.

[31] J. W. Melody, T. Basar, W. R. Perkins, and P. G. Voulgaris, "Parameter identification for inflight detection and characterization of aircraft icing," *Control Engineering Practice*, vol. 8, no. 9, pp. 985–1001, 2000.

[32] Y. Dong and J. Ai, "Research on inflight parameter identification and icing location detection of the aircraft," *Aerospace Science and Technology*, vol. 29, no. 1, pp. 305–312, 2013.

[33] J. W. Melody, T. Hillbrand, T. Basar, and W. R. Perkins, "H^{∞} parameter identification for inflight detection of aircraft icing: the time-varying case," *Control Engineering Practice*, vol. 9, no. 12, pp. 1327–1335, 2001.

[34] Y. Dong and J. Ai, "Inflight parameter identification and icing location detection of the aircraft: the time-varying case," *Journal of Control Science and Engineering*, vol. 2014, Article ID 396532, 11 pages, 2014.

[35] D. Mellinger and V. Kumar, "Minimum snap trajectory generation and control for quadrotors," in *2011 IEEE International Conference on Robotics and Automation*, pp. 2520–2525, Shanghai, China, May 2011.